HYBRID CELLULOSE/GRAPHENE OXIDE NANOCOMPOSITE MEMBRANES FOR WATER DESALINATION

HANANE ABURIDEH, DJAMILA ZIOUI, SARRA HOUT, ZOUBIR BELGROUN, FATMA ZOHRA YAHIAOUI and MOHAMED ABBAS

Unité de Développement des Equipements Solaires, UDES /Centre de Développement des Energies Renouvelables, CDER, Bou Ismail, 42415, W. Tipaza, Algeria
✉ *Corresponding author: H. Aburideh, h_aburideh@yahoo.fr*

Received September 29, 2025

Desalination via reverse osmosis is emerging as a key technology in response to the growing scarcity of freshwater resources. However, conventional membranes still face limitations in terms of durability, fouling, and low ion selectivity. This study aims to develop hybrid membranes based on cellulose acetate (CA), cellulose acetate propionate (CAP), and graphene oxide (GO), in order to simultaneously optimize permeability, thermal stability, and salt retention. The membranes were prepared by phase inversion from polymer formulations incorporating GO, and characterized using FTIR, DSC, filtration tests (pure and saline water), and water absorption measurements. The results demonstrate high chemical compatibility among the components, with the formation of stabilizing hydrogen bonds. The AP-GOf membrane (CA/CAP with functionalized GO) showed the highest permeability (23.75 L/m^2hbar), while the hybrid membrane based on cellulose acetate (CA, 12 wt%), cellulose acetate propionate (CAP, 5 wt%), and graphene oxide (GO) exhibited the best trade-off between water flux (94.32 $L \cdot m^{-2} \cdot h^{-1}$ at 15 bar) and ion retention (70.7% Mg^{2+}, 57% Ca^{2+}, 54.8% NaCl). Increasing the CA content improved selectivity, while the plasticizing effect of CAP and the structuring role of GO enhanced permeability. These findings indicate that fine-tuning the polymer/GO ratios allows tailoring membrane performance to specific needs. In conclusion, the A12%-P5%-GO membrane represents a promising solution for sustainable brackish water desalination, combining effective separation performance with environmental compliance.

Keywords: cellulose acetate, graphene oxide, membranes, water desalination

INTRODUCTION

By 2030, the planet may face an unprecedented water crisis, with global demand exceeding supply by 40%, according to projections by the United Nations.[1] This critical imbalance stems from combined factors: climate change, which disrupts hydrological cycles and intensifies droughts; rapid population growth, which increases demand particularly for agriculture and urban use; and unsustainable resource management, leading to overexploitation and pollution.[1-2] In this context, seawater desalination emerges as a strategic solution to enhance water security, especially in arid and coastal regions. Although this technology is energy-intensive, technical advancements and the integration of renewable energy sources are improving its environmental and economic viability.

Two main desalination methods are commonly used: thermal distillation and, more predominantly, reverse osmosis (RO), which accounts for over 60% of desalination units worldwide.[2-3] Reverse osmosis uses a semi-permeable membrane to extract dissolved salts, offering lower energy consumption compared to thermal processes and compatibility with renewable energy sources. The membrane is therefore a central component, whose performance directly determines the overall efficiency of the process. These membranes are mainly made from synthetic polymers (aromatic polyamide, polysulfone, cellulose acetate).[4] Due to their polymeric nature, such membranes have undergone significant development over the years, particularly with the emergence of composite membranes. Today, thin-film composite (TFC) polyamide membranes dominate the reverse osmosis market thanks to their high salt rejection efficiency (>99%), good permeability, and suitability for small decentralized systems.

However, their vulnerability to biological and chemical fouling has spurred interest in nanotechnologies.[5] The incorporation of nanomaterials into conventional polymer matrices enables the fabrication of more advanced nanomembranes. Materials such as graphene, graphene oxide (GO), carbon nanotubes, metal nanoparticles (Ag, ZnO, TiO_2), and mesoporous silica enhance hydrophilicity, chemical stability, mechanical strength, and antibacterial activity.[6] Furthermore, the limited lifespan of these membranes leads to frequent replacements, increasing both waste and costs.[7] To overcome these limitations, researchers are developing high-performance, biofouling-resistant, and durable membranes incorporating nanomaterials like graphene and metal oxides.[8] Other promising approaches explore bioinspired membranes based on aquaporins or biodegradable polymers, aiming to reduce environmental impact and dependence on petrochemical derivatives.[9] Additionally, recycling of spent membranes is becoming crucial within a circular economy perspective.

Discovered as a two-dimensional material in 2004 by Novoselov and Geim, graphene possesses remarkable properties: impermeability, high thermal conductivity (>2000 W/mK), transparency (97.7%), mechanical strength, high specific surface area (>2600 m^2/g), and exceptional electronic mobility (>200,000 cm^2/Vs).[10] It is applicable to desalination, as illustrated by Martin Lockheed's 2013 “Perforene” patent, which describes a graphene membrane perforated with nanopores. To make these membranes permeable to water, several researchers have introduced pores ranging from 1.5 to 62 $Å^2$ using techniques such as chemical vapor deposition, ion bombardment, or oxidation.[11-12] Nanoporous graphene membranes reported in the literature achieved fluxes of up to 100 $L \cdot cm^{-2} \cdot day^{-1} \cdot MPa^{-1}$ with excellent salt rejection.[13] Gupta *et al*.[16] analyzed the influence of laser parameters on the fabrication of laser-induced graphene (LIG) filters based on polyethersulfone (PES), optimized for water purification (dye removal, disinfection) and interfacial evaporation desalination. They showed that laser power, image density, support nature, and platform influence the porosity and performance of LIG filters. It has been demonstrated that chemical functionalization, pressure, and pore size affect the efficiency of graphene membranes, which are capable of blocking salt ions, while allowing water to pass at high fluxes (10–100 $L \cdot cm^{-2} \cdot day^{-1} \cdot MPa^{-1}$), thanks to their atomic thickness.

Finally, Mallakpour *et al*.[13] emphasized the importance of sustainability in the production of graphene-based nanomembranes, highlighting the need to reduce energy consumption, emissions, and adopt environmentally friendly practices. According to a literature review, many graphene-based composite nanomembranes have demonstrated salt rejection rates of 99.9%. Examples include the Magnesium–Lithium Hydrotalcite superhydrophobic (MLH-0.1) mixed matrix nanofiber membrane, the chitosan/graphene oxide mixed matrix membrane, the Metal–Organic Framework–Graphene Oxide–Polydimethylsiloxane membrane (MOF-GO-PDMS), the TFC GO membrane crosslinked with poly N-isopropylacrylamide–N,N′-methylenebisacrylamide (NIPAM-MBA), the PA-GO composite membrane, and the GO polymer membrane. Among these, the PA-GO composite membrane, fabricated by interfacial polymerization, demonstrated the highest salt rejection of 99.99%, with a water flux of 24.0 $kg \cdot m^{-2} \cdot h^{-1}$. The production of high-quality, defect-free graphene membranes on an industrial scale remains a major challenge that researchers are actively working to overcome.

In parallel, for several decades, research has focused on developing membranes combining high flux and high salt rejection for seawater treatment.[17] Among the most commonly used hydrophilic polymers is cellulose acetate (CA), valued for its low cost, availability, biocompatibility, and moderate chlorine resistance.[18-19] However, its strong hydrophilicity can limit permeate flux due to the formation of a dense layer during phase inversion coagulation.[20] Therefore, modifications are necessary, through blending with other polymers or incorporation of nanomaterials.[21]

In this context, our work aims to develop innovative hybrid membranes for desalination by combining cellulose acetate (CA), cellulose acetate propionate (CAP), and graphene oxide (GO). This formulation leverages the complementary properties of these materials: CA ensures good hydrophilicity, CAP improves chemical and mechanical stability, while GO enhances permeability, ionic selectivity, and fouling resistance. This synergy results in high-performance membranes capable of maintaining high flux, while ensuring optimal salt rejection – essential criteria for sustainable desalination of seawater or brackish water.

EXPERIMENTAL

Materials

In the preparation of cellulose acetate (CA)-based membranes, several chemicals are used to modulate solubility, porosity, and final membrane performance. Acetone (CAS: 67-64-1), acted as the main solvent; its volatility promotes rapid evaporation, forming a dense skin on the membrane surface. N-methyl-2-pyrrolidone (NMP) (CAS: 872-50-4) is a less volatile secondary solvent that facilitates the development of an internal porous structure, essential for forming an asymmetric membrane. Methanol (CAS: 67-56-1) functions as a non-solvent, inducing controlled instability in the solution and promoting pore formation. Meanwhile, acetic acid (CAS: 64-19-7) serves as a plasticizer, reducing the brittleness of the polymer film. All these reagents are commercially available from suppliers such as Sigma-Aldrich, Fisher Scientific, or Carlo Erba. Graphene oxide (GO) was synthesized from natural graphite powder (CAS: 7782-42-5) using a modified Hummers' method.

Membrane preparation

Graphene oxide synthesis

Graphene oxide was synthesized from graphite powder using a modified Hummers' method.[22-23] In a 500 mL flask, 1 g of graphite powder was dispersed in 23 mL of concentrated sulfuric acid (H_2SO_4, 98%). The mixture was placed in an ice bath at 5 °C under continuous stirring for 5 minutes (Fig. 1(a)). Next, 3 g of potassium permanganate ($KMnO_4$) was gradually added to avoid localized exothermic reactions, while maintaining the temperature at 5 °C for 2 hours. The temperature was then gradually increased to 35 °C, and the mixture was stirred vigorously for 30 minutes (Fig. 1(b)). Then, 46 mL of distilled water was slowly added, causing a rapid temperature rise to approximately 98 °C due to the heat of hydration. This temperature was maintained for 30 minutes under agitation. To terminate the reaction, 140 mL of distilled water and 10 mL of hydrogen peroxide (H_2O_2) were added. The addition of H_2O_2 induced a color change to yellow-brown, indicating complete oxidation of graphite (Fig. 1(c)). The solid product was recovered by vacuum filtration and washed five times with 200 mL of 5% hydrochloric acid (HCl) to remove manganese residues (Fig. 1(d)). The solid was then rinsed with hot water (70 °C) to eliminate traces of acid (Fig. 1e). Finally, after several washes, the filtered graphene oxide was dried at 60 °C for 12 hours in air (Fig. 1(f)).

Functionalization of graphene oxide (GO)

A portion of the synthesized graphene oxide (GO) was subjected to functionalization to improve its dispersion and compatibility within polymer matrices. Although GO inherently contains oxygenated functional groups (–OH, –COOH, –O–) that confer some degree of hydrophilicity, it tends to aggregate when incorporated into polymer systems, thereby hindering uniform dispersion.[24] Functionalization addresses this issue by introducing specific chemical moieties that enhance the interfacial compatibility between GO and the polymer matrix, resulting in improved dispersion and structural stability.[25]

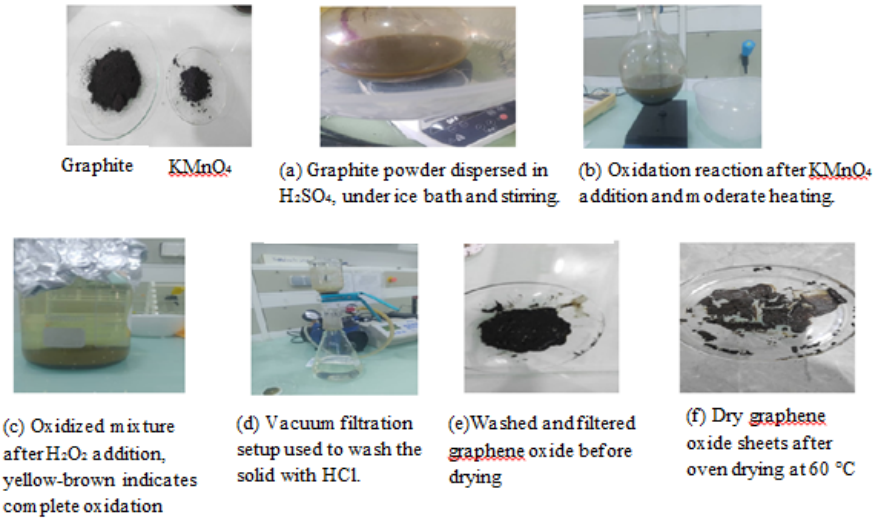

Figure 1: Graphene oxide synthesis via the modified Hummers' method

Additionally, functionalization facilitates the formation of strong intermolecular interaction, such as hydrogen bonding, covalent bonding, or π–π stacking – between GO and the polymer, thereby enhancing the membrane's mechanical strength, durability, and cohesion.[26] Tailoring the surface chemistry of GO through functionalization can also improve its hydrophilicity, water permeability, and resistance to fouling, and may even impart antibacterial properties.[27]

The functionalization process was carried out as follows: a 0.1 wt% dispersion of dry GO was prepared in distilled water and stirred for 30 minutes at room

temperature. A 10 wt% ammonia (NH_3) solution was then added, and the mixture was maintained at 60 °C for 4 hours to facilitate the chemical modification.

Upon completion, the resulting solid was washed three times with distilled water, with each wash followed by filtration; the final filtration step was performed under vacuum. The functionalized GO was then dried at 60 °C for 40 minutes, and finally redispersed in a 17 wt% NMP (N-methyl-2-pyrrolidone) solution, followed by continuous stirring for 24 hours at room temperature to ensure complete dispersion.

Preparation of composite membranes

The membranes were prepared using the non-solvent induced phase separation (NIPS) technique. Three polymer systems were investigated: cellulose acetate (CA), cellulose acetate propionate (CAP), and CA/CAP blends at different ratios. The detailed compositions of the developed membrane formulations are presented in Table 1. The polymers were dissolved in a solvent mixture composed of 100% acetone and 15% N-methyl-2-pyrrolidone (NMP), under stirring at 250 rpm for 4 hours. Then, 1.4 wt% of acetic acid (AA) was added, followed by continuous stirring for 24 hours at room temperature.[28]

In parallel, graphene oxide (GO) solutions were prepared separately by dispersing 0.05 wt% of dry GO in 17% NMP, under stirring at 300 rpm for 24 hours. All solutions were then subjected to sonication: 40 minutes for GO at 25–35 °C, and 15 minutes for the polymer solutions at 30 °C, to ensure homogeneous dispersion and eliminate air bubbles.

GO Incorporation and membrane casting

The functionalized GO solutions were incorporated into the polymer solutions under stirring at 200 rpm for 24 hours, followed by sonication for 15 minutes at 30 °C. The final casting solutions were spread using a 250 µm casting knife onto nonwoven paper, and immediately immersed in a coagulation bath at 5 °C for 10 minutes. The formed films were then transferred to a deionized water bath for one hour, air-dried, and subsequently placed in an oven at 70 °C for 15 minutes. Finally, the membranes were immersed in a distilled water bath containing a few drops of formaldehyde to stabilize their structure.[29] Table 1 summarizes the constituents and composition of the membranes.

Table 1
Composition and constituents of the membranes

Membranes symbol	CA, %	CAP, %	Acetone, %	NMP, %	AA, %	Methanol, %	GO, %	Ammoniac, %
Ac-Go	17	/	100	32	1.4	3.6	0.05	/
CAP-Go	/	17	100	32	1.4	3.6	0.05	/
AP-Go	8.5	8.5	100	32	1.4	3.6	0.05	/
$A_{12\%}P_{5\%}$-GO	12	5	100	32	1.4	3.6	0.05	/
$A_{5\%}P_{12\%}$-GO	5	12	100	32	1.4	3.6	0.05	/
AP-GOf	8.5	8.5	100	32	1.4	3.6	0.05	10
Ac	17	/	100	15	1.4	3.6	0	/
CAP	/	17	100	15	1.4	3.6	0	/

Filtration tests

The experimental setup used for dead-end filtration consists of a laboratory-scale system designed to accommodate flat-sheet membranes with a diameter of 54 mm, providing an effective filtration area of 22.9 cm^2.[30] The system is powered by a high-pressure pump and allows testing under transmembrane pressures ranging from 10 to 30 bar. Continuous stirring ensures homogeneity of the feed solution, while the permeate is collected progressively. Before each initial test, new membranes undergo a conditioning phase involving a gradual pressure increase (in 10-bar increments up to 30 bar) using ultrapure water. This step is intended to compact the membranes without compromising their performance. Filtration experiments were conducted at room temperature, using solutions prepared from neutral or ionic solutes. Given their low concentrations, the solutions were assumed to have a density equivalent to that of water. The entire setup is illustrated in Figure 2.

Characterization

Fourier transform infrared spectroscopy (FTIR)

The synthesized CA/CAP/GO-based polymer membranes were characterized by FTIR spectroscopy. The spectra were recorded using an FTIR spectrophotometer (Agilent Technologies, USA) within the wavelength range of 4000 to 450 cm^{-1}.

Differential scanning calorimetry (DSC)

The glass transition temperatures (Tg) of all flat-sheet membranes were determined using differential scanning calorimetry (DSC) and thermogravimetric analysis (TGA) with a Universal V4.5A TA Instruments system. All thermograms were recorded over a temperature range of 50 °C to 400 °C under a nitrogen atmosphere, using two consecutive heating and cooling cycles at a rate of 10 °C/min. Three samples of each membrane, weighing between 5 and 10 mg, were analyzed.

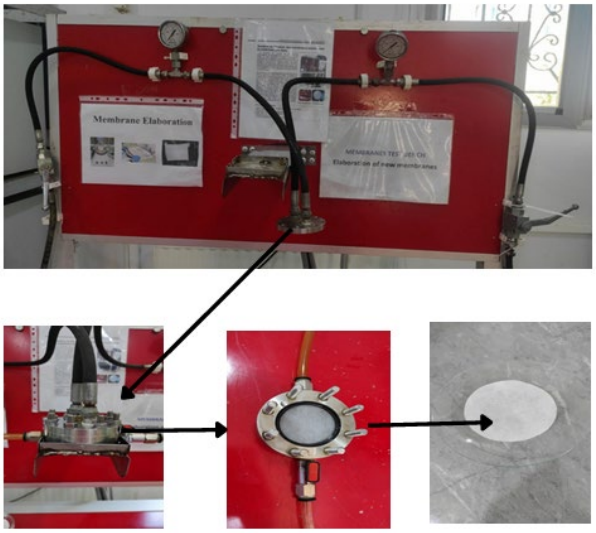

Figure 2: Filtration test setup

Filtration performance test

Selectivity is a key but challenging property to quantify, governed by the physical and chemical nature of the membrane surface.[31] It reflects the membrane's ability to retain specific dissolved species and is generally expressed as the rejection rate (T_R). In reverse osmosis, this parameter is commonly evaluated using sodium chloride (NaCl) as a reference solute, particularly in water demineralization processes.

The membranes were tested using synthetic saline water with a concentration of approximately 11 g/L, representative of the brackish groundwater typically found in southern Algerian aquifers, as well as real-source water from the Mediterranean Sea (Tipaza, located west of Algiers), characterized by a pH of 7.4, a conductivity of 53.2 mS/cm, and a salinity of 32.7 g/L. The observed rejection rate (T_R) is experimentally determined using the following formula:

$$T_R = 1 - \frac{C_p}{C_a} \quad (1)$$

where C_a is the solute concentration in the feed solution (mg/L), C_p is the solute concentration in the permeate (mg/L).

Water absorption/water content

As part of the experiments, the study of water absorption-based wettability was conducted to assess the hydrophilic or hydrophobic nature of the fabricated membranes. The membrane films were immersed in water for 24 hours, then wiped and weighed to obtain the wet weight. Subsequently, they were dried at 80 °C for 24 hours to determine the dry weight. This method enabled the evaluation of the membranes' water absorption capacity by calculating the percentage of water uptake based on the variation in mass:

$$\text{Water absorption (\%)} = \frac{Mh - Ms}{Mh} \times 100 \quad (2)$$

where Mh is wet membrane weight (g), Ms – dry membrane weight (g).

RESULTS AND DISCUSSION

Fourier transform infrared spectroscopy (FTIR)

The FTIR analysis of CA/CAP/GO composite membranes reveals specific interactions between the constituents, confirming the successful incorporation of graphene oxide (GO) into the polymer matrix (Fig. 3). In the 1400–400 cm^{-1} region, the characteristic bands of cellulose derivatives are clearly observed (C–O at ~1190 and ~1035 cm^{-1}, and $–CH_3$ at 1375 cm^{-1}), with increased intensity due to the presence of CAP. GO exhibits typical absorption bands associated with oxidized functional groups, such as C–O–C (~1220–1250 cm^{-1}), C–O (1050–1100 cm^{-1}), and the graphitic skeleton (500–600 cm^{-1}), indicating a high oxidation level.[32]

The incorporation of GO induces notable spectral changes, including a shoulder at ~1269 cm^{-1} and intensified bands in the 1050–1100 cm^{-1} region, reflecting improved structural organization and enhanced polymer–GO interactions. In the 1600–2000 cm^{-1} range (Fig. 4), a shift of the C=O band to 1739 cm^{-1} along with broadening suggests the formation of hydrogen bonds between ester carbonyl groups and GO functional groups. Moreover, the attenuation of the band at 1623 cm^{-1} (C=C sp^2 from GO) indicates π–π interactions or hydrogen bonding with the polymer matrix.[32-33] In the 2800–3600 cm^{-1} region, broadening of

aliphatic C–H and O–H bands further confirms hydrogen bonding between polymer chains and the hydroxyl or carboxyl groups of GO.

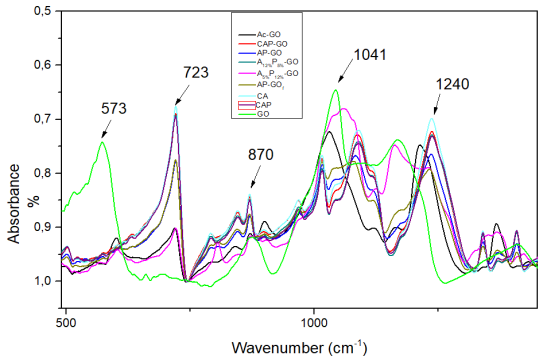

Figure 3: FTIR spectra of the membranes in the range of 500–1500 cm⁻¹

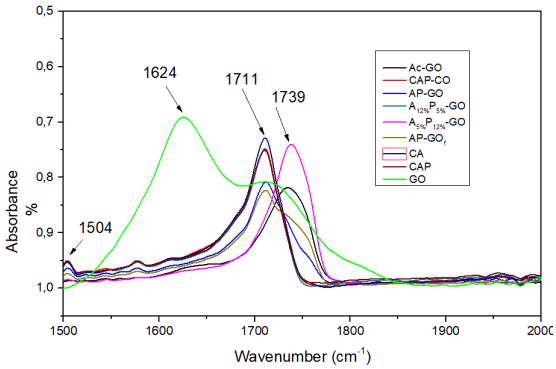

Figure 4: FTIR spectra of the membranes in the range of 1500–2000 cm⁻¹

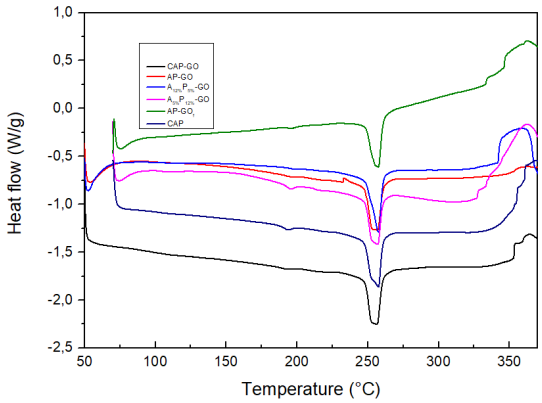

Figure 5: DSC curves of the membranes in the temperature range 200–400 °C

These spectral observations confirm good compatibility among the components and the formation of stable intermolecular interactions, establishing a strong structural foundation for optimizing the physicochemical properties of the membranes.[34]

Differential scanning calorimetry (DSC)

Differential scanning calorimetry (DSC) is a commonly used technique to evaluate the thermal behavior of polymers, particularly blends, by measuring heat flow as a function of temperature. It provides essential data, such as the glass transition temperature (Tg), melting temperature (Tm), and crystallization temperature (Tc).[35] CA/CAP/GO-based membranes were analyzed in the temperature range of 50 °C to 400 °C with a heating rate of 10 °C/min.

As shown in Figure 5, for the CAP-GO membrane, the characteristic temperatures observed were Tg ≈ 192 °C, Tm ≈ 257 °C, and Tc ≈ 354 °C. These values correspond respectively to the material softening, the melting of crystalline regions, and a cold crystallization phenomenon. A pure CAP membrane shows very similar temperatures (Tg = 192 °C, Tm = 257 °C, Tc = 355 °C), but exhibits a higher heat flow, indicating a more crystalline structure. The introduction of GO reduces this thermal flow due to the formation of hydrogen bonds between the functional groups of GO (–OH, –COOH) and those of CAP (–OH, acetate, propionate), which limits the mobility of polymer chains and their ability to crystallize.[36]

The AP-GO membrane shows similar temperatures (Tg = 192 °C, Tm = 255 °C, Tc = 355 °C), while the cellulose acetate (CA)/cellulose acetate propionate (CAP) blend membrane incorporating ammonia-functionalized graphene oxide (GOf), hereafter referred to as the AP-GOf membrane, exhibits slightly higher values: Tg = 195 °C, Tm = 257 °C, and Tc = 363 °C. This increase, particularly in Tc, is attributed to the presence of amine groups (–NH_2), which can form additional hydrogen bonds with the functional

groups on both A and CAP polymers, thus reinforcing the structure. The higher thermal flow observed in the AP-GOf membrane reflects a more pronounced crystalline organization compared to AP-GO.

Finally, the mixed membranes named A12%-P5%-GO and A5%-P12%-GO show Tg = 200 °C, Tm = 258 °C, Tc = 342 °C and Tg = 194 °C, Tm = 254 °C, Tc = 329 °C, respectively. The membrane enriched in cellulose acetate (A12%) exhibits a higher heat flow, suggesting a more ordered structure. Cellulose acetate, which is richer in hydroxyl groups than CAP, promotes the formation of hydrogen bonds with GO, enhancing membrane crystallinity. Conversely, CAP, being more flexible and less hydroxylated, limits this thermal structuring capacity.

In summary, DSC analysis confirms the influence of polymer composition and the presence of GO (functionalized or not) on the thermal properties of the membranes. A higher content of cellulose acetate or functionalized GO increases crystallinity and thermal stability, whereas CAP or unmodified GO tends to make the structure more amorphous.[35-36]

Pure water flux (PWF) study

The analysis of pure water permeability (PWP) provides insight into the membranes' ability to allow water to pass through in the absence of solutes an essential parameter for assessing their performance. Measurements were conducted at different pressures (10 to 30 bar), and the results presented in Figure 6 show a progressive stabilization of water flux over time.

Virgin membranes based on cellulose acetate (CA) and cellulose acetate propionate (CAP) exhibited initial fluxes of 450 and 520 $Lm^{-2}h^{-1}$, respectively, under 10 bar. This behavior is attributed to the inherent porosity of these unmodified polymers. The higher flux observed for CAP is due to its more flexible and less dense chemical structure compared to CA, resulting from its long side chains and plasticizing effect.

The addition of graphene oxide (GO) generally enhances the water flux of composite membranes by increasing hydrophilicity and creating preferential transport pathways. However, this improvement is not observed in the A12%P5%-GO membrane, where the high CA content leads to a more rigid and compact structure, reducing permeability. This lower performance is further exacerbated by the low CAP content limiting the plasticizing effect and by GO polymer interactions that densify the matrix, consistent with DSC results.

The highest performances were observed for the AP-GOf (~670 $Lm^{-2}h^{-1}$) and A5%CAP12%GO (~630 $L/m^2.h$) membranes. In AP-GOf, the presence of ammonia-functionalized GO (GOf) improves dispersion and compatibility with the CA/CAP matrix, enhancing hydrophilicity and structural openness. The balanced ratio between the rigidity of CA and the flexibility of CAP also contributes to high permeability. In A5%CAP12%GO, the high CAP content increases porosity through its plasticizing action. Although the GO used in this formulation is not reduced, it still contributes to the structuring and hydrophilic surface of the membrane.

A comparison between A12%P5%-GO, A5%P12%-GO, and AP-GOf highlights the importance of the CA/CAP ratio. A higher CAP content, as in A5%P12%-GO and AP-GOf, promotes higher water flux and better pressure stability. Although the incorporation of 0.05 wt% GO generally improves permeability, its effectiveness is strongly dependent on the polymer composition. Across all tested pressures (15 to 30 bar), the trend in the flux curves remained consistent among the different formulations, confirming the reproducibility of the results.

The hydraulic permeability (Lp) is a key indicator of membrane performance, reflecting the ease with which water passes through under a pressure gradient. Closely related to flux, higher Lp values generally indicate a greater capacity for water transport. In this study, the AP-GOf membrane exhibited the best permeability, with an Lp value of 23.75 L/m^2hbar. This performance is attributed to the use of functionalized GO (GOf), obtained via partial ammonia reduction. This chemical modification reduces the –COOH groups in favor of –OH, which improves material hydrophilicity, limits nanosheet aggregation, and allows for homogeneous dispersion within the polymer matrix. As a result, GOf promotes the formation of well-organized channel networks that facilitate water transport while maintaining good structural stability.[37-39]

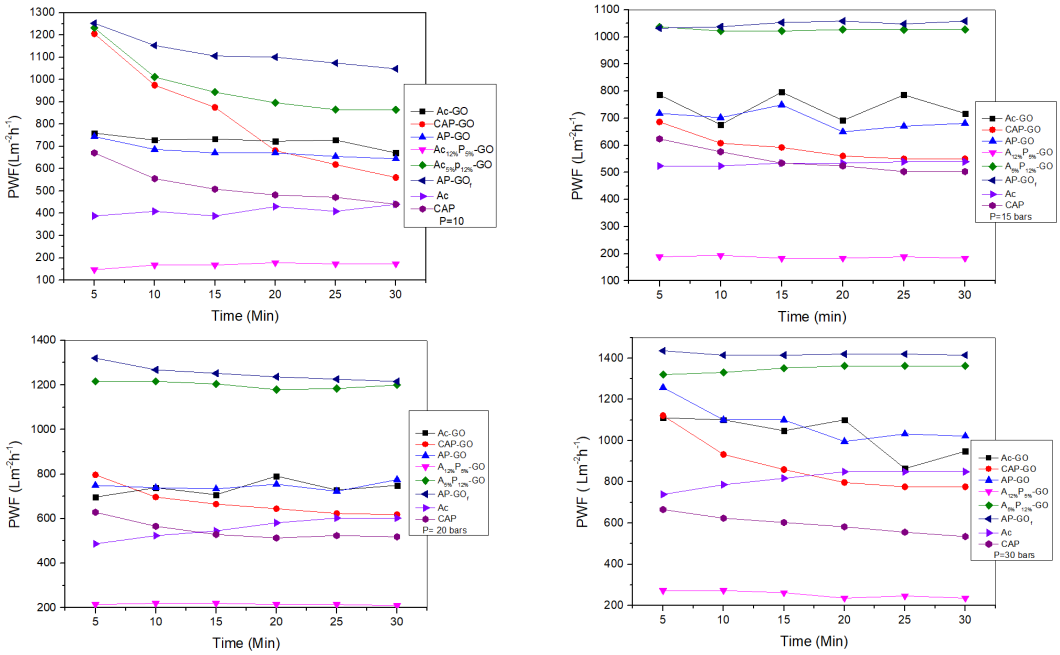

Figure 6: Variation of pure water flux PWF over time for all the membranes

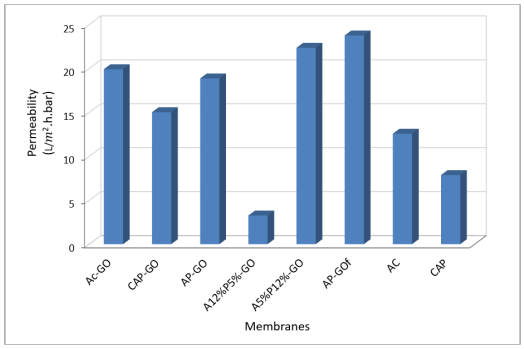

Figure 7: Hydraulic permeability of all the membranes

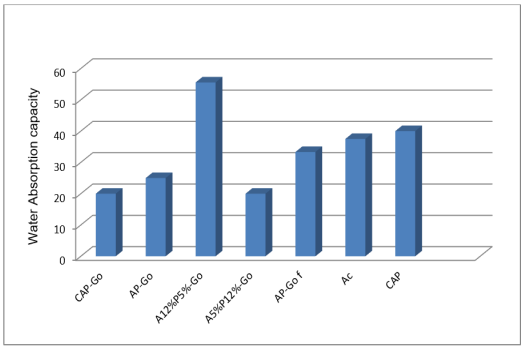

Figure 8: Water absorption of all the membranes

In contrast, the A12%P5%-GO and CAP membranes showed lower permeabilities of 3.26 and 7.86 L/m^{2}hbar, respectively, as illustrated in Figure 7. These poor performances are likely due to incomplete GO dispersion, leading to nanosheet aggregation and partial blockage of flow pathways. Although these membranes are capable of absorbing water, their compact structure and lack of efficient channels limit water passage. Gao *et al.*[40] demonstrated that while GO improves hydrophilicity, poor dispersion can adversely affect permeability. Similarly, Shen *et al.*[41] observed that highly crosslinked membranes, although absorbent, may exhibit low water permeability.

Nevertheless, in CA/CAP membranes incorporating non-functionalized GO, a flux improvement was still observed. When well-dispersed, GO acts as a structuring agent, forming preferential transport channels within the matrix. It also increases the overall hydrophilicity of the membrane, which enhances water uptake and transport under pressure.

Water absorption capacity

Water absorption capacity is a key indicator of membrane wettability, revealing its hydrophilic or hydrophobic character. This property directly influences membrane behavior in aqueous environments, particularly the interaction with water and overall performance.

The results shown in Figure 8 indicate that membranes rich in cellulose acetate – such as A12%-P5%-GO and pure CA – exhibit the highest

water absorption rates, reaching 55% and 40%, respectively. This strong hydrophilicity is attributed to the abundance of hydroxyl (–OH) groups in the acetate structure, which promote hydrogen bonding with water molecules. In contrast, membranes with a high content of cellulose acetate propionate (CAP), such as CAP and CAP-GO, exhibit lower water absorption levels (20–30%), reflecting their more hydrophobic nature due to higher substitution of –OH groups.[42]

Hybrid membranes such as AP-GO and AP-GOf, composed of equal parts CA and CAP, show intermediate water absorption values (25–34%), but demonstrate the highest water permeabilities. This observation highlights that permeability is not solely determined by overall hydrophilicity, but also by the internal structure of the membrane. A well-balanced structure between rigidity and flexibility, combined with a favorable alignment of GO nanosheets and their functional groups (–OH, –COOH, epoxy), facilitates rapid water transport despite moderate absorption levels.[43]

Paradoxically, the A12%-P5%-GO membrane, although highly hydrophilic, shows the lowest permeability. This apparent contradiction is explained by its dense and highly crosslinked internal structure, which, while capable of retaining water, restricts its diffusion through the membrane. This confirms that high water uptake does not necessarily guarantee high permeability, as water transport is strongly influenced by the microstructure of the polymer network.

Tested membrane permeability to synthetic saline water

Figure 9 presents the evolution of water flux during the filtration of synthetic saline water under a constant pressure of 15 bar. Overall, the fluxes remain relatively stable over time, showing trends similar to those observed with pure water. The A_{12}%-P_5%-GO membrane exhibits relatively low flux values, ranging from approximately 130 to 160 $L \cdot m^{-2} \cdot h^{-1}$, which remain lower than those of most GO-modified hybrid membranes such as AP-GO, CAP-GO, and A_5%-P_{12}%-GO. However, its flux is higher than that of the pristine CA membrane (AC), which shows the lowest flux values, ranging from approximately 82 to 90 $L \cdot m^{-2} \cdot h^{-1}$.

In contrast, the highest flux is observed for the AP-GOf and A_5%-P_{12}%-GO membranes, reaching approximately 1130 and 980 $L \cdot m^{-2} \cdot h^{-1}$, respectively. These membranes maintain high and stable flux throughout the filtration period, indicating enhanced permeability in saline conditions. This improved performance can be attributed to the presence of GO and the optimized CA/CAP ratio, which enhance membrane hydrophilicity, promote water transport, and improve structural properties.[44-45]

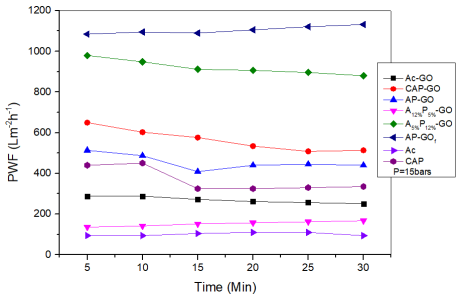

Figure 9: Variation of synthetic saline water flux over time for all the membranes

Furthermore, the incorporation of GO/CAP and the balanced polymer composition contribute to improved resistance to fouling and reduced pore blockage. Hydrophilic functional groups facilitate water diffusion while limiting salt accumulation on the membrane surface. This favorable combination of hydrophilicity, structural stability, and optimized pore structure promotes efficient and stable water transport even in the presence of dissolved salts.

Salt retention

Figure 10 illustrates the retention of synthetic saline solutions for all membranes. Overall, all membranes demonstrated good effectiveness against divalent ions, particularly calcium (Ca^{2+}) and magnesium (Mg^{2+}) ions, with retention rates ranging from 38.9% to 56.5% for Ca^{2+} and 47.8% to 70.7% for Mg^{2+} ions. The A12%-P5%-GO membrane exhibited the best performance for Mg^{2+}

(70.7%), while the pure CA membrane showed the highest retention rate for Ca^{2+} ions (60%).

For the monovalent salt NaCl, membranes displayed highly variable behaviors. The A12%-P5%-GO membrane achieved the highest retention (54.8%), whereas the A5%-P12%-GO membrane recorded the lowest (20.9%). This variability highlights the influence of chemical composition and membrane structure on ionic selectivity.

The results confirm that membranes with a high cellulose acetate (CA) content are more effective in separating divalent ions (Mg^{2+}, Ca^{2+}) from NaCl. The descending order of NaCl rejection was as follows: A12%-P5%-GO > CA > CA-GO > AP-GO > AP-GOf > CAP-GO ≈ CAP > A5%-P12%-GO.

A comparative bar chart reveals that pure CA membranes provide better rejection capabilities (Ca^{2+}: 60%, Mg^{2+}: 64.6%, NaCl: 52.2%) than pure CAP membranes (Ca^{2+}: 40%, Mg^{2+}: 52.6%, NaCl: 26.1%). This difference is attributed to the denser and more polar structure of CA, which favors both size exclusion and electrostatic interactions.

However, incorporating GO into CA membranes results in reduced salt retention (Ca^{2+}: 46%, Mg^{2+}: 56.2%, NaCl: 43.1%). This decrease may be due to the formation of nanoscopic channels between GO nanosheets, which increase permeability and facilitate ion diffusion, especially for monovalent species. Additionally, interactions between GO functional groups and those of CA may disrupt the internal membrane structure, diminishing its separation capability.

In contrast, the addition of GO to CAP membranes did not significantly improve salt retention performance. Retention rates for the CAP-GO membrane (Ca^{2+}: 43%, Mg^{2+}: 49.4%, NaCl: 26.1%) remained close to those of pure CAP, suggesting that GO mainly enhances permeability without substantially impacting selectivity. Furthermore, membranes with a CAP/CA ratio ≥1 generally exhibited lower rejection rates. This trend could be attributed to increased surface porosity in CAP-rich membranes, which facilitates water transport but limits ion exclusion. Thus, although GO improves wettability and flux, its effect on salt rejection remains limited in CAP-dominant formulations.

Conversely, among hybrid membranes composed of CA, CAP, and GO, the A12%-P5%-GO formulation containing a high CA content (12%) and a low CAP content (5%) demonstrated the best overall salt rejection performance, achieving 57% for Ca^{2+}, 70.7% for Mg^{2+}, and 54.8% for NaCl, with a moderate flux of 94.32 $L/m^2.h$ under 15 bar. These results, which surpass those of pure CA membranes, indicate that this composition offers an optimal balance between permeability and selectivity, benefiting from the rigid structure of CA, the plasticizing effect of CAP, and the structuring influence of GO.

Selective ion separation was also tested using real seawater from Fouka, characterized by a pH of 7.4, conductivity of 53.2 mS/cm, and salinity of 32.7 g/L. The results shown in Figure 11 indicate that the developed membranes retained divalent cations (Mg^{2+} and Ca^{2+}) more effectively than monovalent salts (NaCl), due to size exclusion based on the hydrated radius of the ions. Membranes rich in CA, such as pure CA and A12%-P5%-GO, delivered the best overall performance, reaching up to 64% retention for Mg^{2+} ions and 55% for NaCl. This efficiency is attributed to their dense structure and the presence of acidic functional groups (–OH, –COOH) from GO, inducing a Donnan effect that enhances electrostatic exclusion.[46-48]

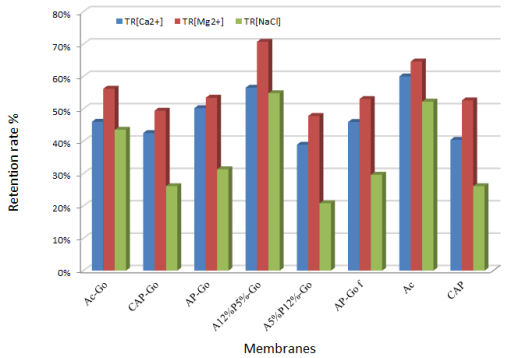

Figure 10: Salt rejection performance of all tested membranes with synthetic saline water

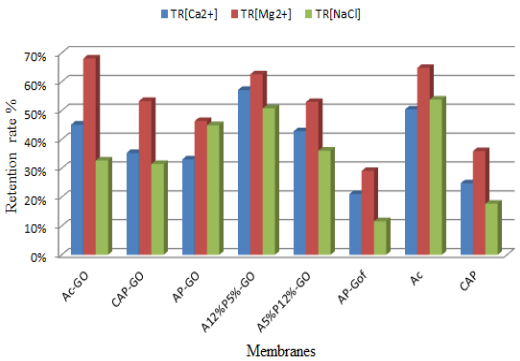

Figure 11: Salt rejection rates of all tested membranes with Fouka seawater

In contrast, the AP-GOf membrane, although highly permeable, exhibited the lowest retention rates (NaCl ≈ 15%), suggesting that excessive GO functionalization can disrupt the membrane structure and reduce selectivity. Hybrid membranes containing CAP outperformed pure CAP (Ca^{2+}: 24.81%, Mg^{2+}: 35.94%, NaCl: 17.74%), confirming the beneficial effects of CA and GO addition. This synergy allows for the adjustment of density, pore size, and hydrophilicity, thereby optimizing separation performance.

Nevertheless, despite these improvements, NaCl rejection remains insufficient to meet WHO salinity standards. The descending order of NaCl rejection was:

CA > A12%-P5%-GO > AP-GO > A5%-P12%-GO > CA-GO > CAP-GO > CAP > AP-GOf.

Ultimately, the A12%-P5%-GO membrane stands out with optimal performance, combining a flux of 94.32 $Lm^{-2}h^{-1}$ at 15 bar with retention rates of 68.59% for Mg^{2+}, 61.14% for Ca^{2+}, and 54.82% for NaCl. It thus meets WHO guidelines for divalent ions, offering promising potential for hard water treatment and partial desalination of brackish water. These findings confirm that in the context of nanofiltration, the rejection of monovalent salts remains a significant limitation.

CONCLUSION

The main objective of this work was to design nano-modified hybrid membranes by combining the film-forming properties of cellulose acetate propionate (CAP) with the dense structure of cellulose acetate (CA), while incorporating graphene oxide (GO) as a hydrophilic nanomaterial. This approach was intended to achieve an optimal balance between water flux, hydraulic permeability, and ion retention by tailoring the structure of a cellulosic matrix fabricated via phase inversion.

FTIR analyses confirmed the homogeneous incorporation of the components, revealing characteristic bands and the formation of hydrogen bonds, indicating good compatibility between the polymers and GO. The AP-GOf membrane, which included functionalized GO, stood out with its high permeability (23.75 L/m^2hbar) and impressive initial flux (670 $L/m^2.h$ at 10 bar), attributed to homogeneous dispersion of GOf and a well-balanced structure between flexibility and rigidity.

The wettability study showed that membranes with high CA content had higher water absorption capacity, though this did not necessarily translate into greater permeability – an observation highlighting the influence of matrix density and microstructure on transport properties. DSC thermal analysis revealed the impact of the CA/CAP ratio and the chemical nature of GO on the crystallinity and thermal stability of the membranes, directly affecting their structural performance.

The A_{12}%-P_5%-GO hybrid membrane exhibits a significantly higher flux than the pure CA membrane, confirming the beneficial effect of GO incorporation and the CA/CAP blend. These results highlight the importance of optimizing polymer composition to develop high-performance and durable membranes for desalination.

In terms of salt retention, the A12%-P5%-GO membrane demonstrated the best selective performance: 70.7% for Mg^{2+}, 57% for Ca^{2+}, and 54.8% for NaCl in synthetic solution. Its effectiveness was also confirmed with real seawater from Fouka, with respective rejection rates of 68.59%, 61.14%, and 54.8%, and a moderate flux of 94.32 $Lm^{-2}h^{-1}$. This overall performance is attributed to its structure reinforced by the controlled incorporation of CAP and GO.

REFERENCES

[1] United Nations, World Water Development Report: Water for a Sustainable World, UNESCO Publishing, Paris, 2015

[2] A. Al-Karaghouli and L. L. Kazmerski, *Renew. Sustain. Energ. Rev.*, **13**, 1182 (2009), https://doi.org/10.1126/science.1200488

[3] M. Elimelech and W. A. Phillip, *Science*, **333**, 712 (2011), https://doi.org/10.1126/science.1200488

[4] K. Guan, Y. Sasaki, Y. Jia, R. Gonzales and P. Zhang, *J. Membr. Sci.*, **640**, 119801 (2021), https://doi.org/10.1016/j.memsci.2021.119801

[5] M. Shabin, A. Jamaliah and H. Raed, *Chemosphere*, **363**, 142927 (2024), https://doi.org/10.1016/j.chemosphere.2024.142927

[6] A. Lee, J. W. Elam and S. B. Darling, *Environ. Sci.: Water Res. Technol.*, **6**, 290 (2011), https://doi.org/10.1039/C9EW00954A

[7] A. Ali, S. Ahmed and M. Rizwan, *J. Membr. Sci.*, **634**, 119405 (2021), https://doi.org/10.1016/j.memsci.2021.119405

[8] L. F. Greenlee, D. F. Lawler, B. D. Freeman, B. Marrot and P. Moulin, *Water Res.*, **43**, 2317 (2009), https://doi.org/10.1016/j.watres.2009.03.010

[9] A. Boretti, S. Al-Zubaidy, M. Vaclavikova, M. Al-Abri, S. Castelletto *et al.*, *Clean Water*, **1**, 5 (2018), https://doi.org/10.1038/s41545-018-0004-z

[10] J. S. Bunch, S. S. Verbridge, J. S. Alden, A. M. Van Der Zande, J. M. Parpia *et al*., *Nano Lett*., **8**, 2458 (2008), https://doi.org/10.1021/nl801457b
[11] M. E. Suk and N. R. Aluru, *J. Phys. Chem. Lett*., **1**, 1590 (2010), https://doi.org/10.1021/jz100240r
[12] S. Mallak, and C. M. Hussain (Eds.), "Environmental Applications of Carbon Nanomaterials-Based Devices", Wiley-VCH, 2021, https://doi.org/10.1002/9783527825565
[13] K. E. Whitener and P. E. Sheehan, *Diamond Relat. Mater*., **46**, 25 (2014), https://doi.org/10.1016/j.diamond.2014.04.006
[14] M. Lotya, Y. Hernandez, P. J. King, R. J. Smith, V. Nicolosi *et al*., *J. Am. Chem. Soc*., **131**, 3611 (2009), https://doi.org /10.1021/ja807449u
[15] R. S. Gupta, S. Mandal, A. Malakar, S. Rege, S. S. Islam *et al*., *J. Mater. Chem. A*, **12**, 321 (2024)
[16] J. R. Werber, C. O. Osuji and M. Elimelech, *Nat. Rev. Mater*., **1**, 16018 (2016), https://doi.org/10.1038/natrevmats.2016.18
[17] A. Srivastava, R. Singh, V. D. Rajput, T. Minkina, S. Agarwal *et al*., *Chemosphere*, **303**, 135230 (2022), https://doi.org/10.1016/j.chemosphere.2022.135230
[18] J. J. Peirce, R. F. Weiner and P. A. Vesilind, in "Environmental Pollution and Control", 4th Ed., Butterworth-Heinemann, Elsevier, 1998, https://doi.org/10.1016/B978-0-7506-7083-2.X5000-9
[19] S. Ahuja, "Handbook of Water Purity and Quality", Academic Press, 2021, https://doi.org/10.1016/B978-0-12-821057-0.00001-7
[20] T. Tomai, S. Ishiguro, N. Tamura, Y. Nakayasu and I. Honma, *Langmuir*, **33**, 5406 (2017), https://doi.org/10.1021/acs.langmuir.7b00434
[21] W. S. Hummers and R. E. Offeman, *J. Am. Chem. Soc*., **80**, 1339 (1958), https://doi.org/10.1021/ja01539a017
[22] D. C. Marcano, D. V. Kosynkin, J. M. Berlin, A. Sinitskii, Z. Sun *et al*., *ACS Nano*, **4**, 4806 (2010), https://doi.org/10.1021/nn1006368
[23] D. R. Dreyer, S. Park, C. W. Bielawski and R. S. Ruoff, *Chem. Soc. Rev*., **39**, 228 (2010), https://doi.org/10.1039/B917103G
[24] J. Shen, Y. Hu, C. Li, C. Qin and M. Ye, *Langmuir*, **25**, 6122 (2009), https://doi.org/10.1021/la900905h
[25] H. Kim, A. A. Abdala and C. W. Macosko, *Macromolecules*, **43**, 6515 (2010), https://doi.org/10.1021/ma 100572e
[26] H. Bai, C. Li, X. Wang and G. Shi, *Chem. Commun*., **13**, 1667 (2010), https://doi.org/10.1039/B917705A
[27] H. Aburideh, D. Zioui, S. Hout, Z. Belgron, F. Z. Yahiaoui *et al*., *Cellulose Chem. Technol*., **59**, 29 (2025), https://doi.org/10.35812/CelluloseChemTechnol.2025.59.03
[28] S. Zinadini, A. A. Zinatizadeh, M. Rahimi, V. Vatanpour and H. Zangeneh, *J. Membr. Sci*., **453**, 292 (2014), https://doi.org/10.1016/j.memsci.2013.11.023
[29] H. Aburideh, N. Kasbadji, M. W. Naceur, Z. Tigrine, D. Tassalit *et al*., *Cellulose Chem. Technol*., **53**, 583 (2019), https://doi.org/10.35812/CelluloseChemTechnol.2019.53.58
[30] S. Shanmuganathan, P. Loganathan, C. Kazner, M. A. H. Johir and S. Vigneswaran, *Desalination*, **403**, 187 (2017), https://doi.org/10.1016/j.desal.2016.06.022
[31] N. Kumar, B. Kumar, H. Gupta and A. Kumar, *Polymers*, **15**, 572 (2023), https://doi.org/10.3390/polym1530572
[32] Y. Miao, X. Wang, Y. Liu, Z. Liu and W. Chen, *Polymers*, **13**, 4453 (2021), https://doi.org/10.3390/polym13244453
[33] H. Aburideh, Z. Tigrine, L. Aoudjit, Z. Belgroun, K. Redjimi *et al*., *Cellulose Chem. Technol*., **55**, 1153 (2021), https://doi.org/10.35812/CelluloseChemTechnol.2021.55.99
[34] H. R. Chae, J. Lee, C. H. Lee, I. C. Kim and P. K. Park, *J. Membr. Sci*., **483**, 128 (2015), https://doi.org/10.1016/j.memsci.2015.02.012
[35] G. Liu, W. Jin and N. Xu, *Chem. Soc. Rev*., **44**, 5016 (2015), https://doi.org/10.1039/C5CS00201J
[36] J. Shen, G. Liu, K. Huang, W. Jin, K. R. Lee *et al*., *Angew. Chem. Int. Ed*., **54**, 578 (2015), https://doi.org/10.1002/anie.201409957
[37] J. Lee, H. R. Chae, Y. J. Won, K. Lee, C. H. Lee *et al*., *J. Membr. Sci*., **448**, 223 (2013), https://doi.org/10.1016/j.memsci.2013.08.017
[38] W. G. Osiris and T. H. M. Manal, *Nat. Sci*., **4**, 568 (2012), https://doi.org/10.4236/ns.2012.410076
[39] G. S. Gao, J. Li, Z. Wang and J. Wang, *ACS Appl. Mater. Interfaces*, **9**, 13487 (2017), https://doi.org/10.1021/acsami.7b01938
[40] J. Shen, G. Liu, K. Huang, Q. Li and W. Jin, *Nat. Nanotechnol*., **11**, 643 (2016), https://doi.org/10.1038/nnano.2016.6
[41] H. Aburideh, Z. Tigrine, D. Zioui, S. Hout, L. Aoudjit *et al*., *Cellulose Chem. Technol*., **57**, 911 (2023), https://doi.org/10.35812/CelluloseChemTechnol.2023.57.80
[42] F. Perreault, A. F. de Faria and M. Elimelech, *Chem. Soc. Rev*., **44**, 5861 (2015), https://doi.org/10.1039/C5CS00410A
[43] N. Akther, N. A. Khan and J. Park, *RSC Adv*., **10**, 14356 (2020), https://doi.org/10.1039/D0RA00133H
[44] B. Wang, H. Lin, X. Guo and P. Bai, *Desalination*, **347**, 39 (2014), https://doi.org/10.1016/j.desal.2014.05.035
[45] C. Y. Tseng, Y. S. Ye, M. Y. Cheng, K. Y. Kao, W. C. Shen *et al*., *Adv. Energ. Mater*., **1**, 1220 (2011), https://doi.org/10.1002/aenm.201100244
[46] Q. Liu and G. R. Xu, *Desalination*, **394**, 162 (2016), https://doi.org/10.1016/j.desal.2016.05.008
[47] H. Aburideh, D. Zioui, S. Hout, Z. Belgroun, F.-Z. Yahiaoui *et al*., *Cellulose Chem. Technol*., **59**, 29 (2024), https://doi.org/10.35812/CelluloseChemTechnol.2024.58.100